HAL
open science

Anisotropy and Clausius-Clapeyron relation for forward and reverse stress-induced martensitic transformations in polycrystalline NiTi thin walled tubes

Estephanie Nobre Dantas Grassi, Grégory Chagnon, Henrique Martinni Ramos de Oliveira, Denis Favier

To cite this version:

Estephanie Nobre Dantas Grassi, Grégory Chagnon, Henrique Martinni Ramos de Oliveira, Denis Favier. Anisotropy and Clausius-Clapeyron relation for forward and reverse stress-induced martensitic transformations in polycrystalline NiTi thin walled tubes. Mechanics of Materials, 2020, 146, 10.1016/j.mechmat.2020.103392 . hal-02537803v2

HAL Id: hal-02537803

https://hal.science/hal-02537803v2

Submitted on 14 Apr 2020

HAL is a multi-disciplinary open access archive for the deposit and dissemination of scientific research documents, whether they are published or not. The documents may come from teaching and research institutions in France or abroad, or from public or private research centers.

L'archive ouverte pluridisciplinaire **HAL**, est destinée au dépôt et à la diffusion de documents scientifiques de niveau recherche, publiés ou non, émanant des établissements d'enseignement et de recherche français ou étrangers, des laboratoires publics ou privés.

Anisotropy and Clausius-Clapeyron relation for forward and reverse stress-induced martensitic transformations in polycrystalline NiTi thin walled tubes

Estephanie Nobre Dantas Grassi[a], Grégory Chagnon[a], Henrique Martinni Ramos de Oliveira[a], Denis Favier[a,*]

[a] *Univ. Grenoble Alpes, CNRS, Grenoble INP, TIMC-IMAG, F-38000 Grenoble, France*

Abstract

Inside the Clausius-Clapeyron regime, transformation stresses during superelastic tensile tests of polycrystalline shape memory alloys are linearly dependent on temperature, with coefficients being the slopes of the forward and reverse transformation lines. In this work, experiments are performed to investigate the anisotropy of the slopes of the forward and reverse transformation stress-temperature lines in a NiTi superelastic thin walled tube. The classical Clausius-Clapeyron relation is widely used to model these slopes, although, in a strict sense, this relation is defined at thermodynamic equilibrium. Experimental results disagree with the widely used classical Clausius-Clapeyron relation in two points: (i) that there should be no difference between slopes for forward and reverse transformations and (ii) that the products of the slopes by the transformation strains should not depend on orientation, since the remaining terms (mass density and entropy change) are not orientation dependent. A modified "Clausius-Clapeyron" relation is then proposed, better suited to model the anisotropy of the slopes of stress-temperature transformation lines of forward and reverse in superelastic NiTi. This modification is based on a unified thermodynamic theory of thermoelastic martensitic transformation in which irreversible energies are accounted as a sum of stored elastic energy and

*Corresponding author
Email address: denis.favier@univ-grenoble-alpes.fr (Denis Favier)

dissipated energy. The modified "Clausius-Clapeyron" relation is obtained by expressing that this irreversible energy is temperature dependent and that this temperature dependence is dependent on the orientation.

Keywords: NiTi, superelasticity, temperature dependence, Clausius-Clapeyron, anisotropy

1. Introduction

Superelastic NiTi shape memory alloys (SMA) have the ability to recover strains of the order of 10% in tension by simple mechanical unloading. With a high work output density [1] and a mechanical behaviour compatible with human tissues [2], NiTi superelastic SMA are being applied from engineering systems to biomedical implants. The remarkable amount of recoverable strain is attained through a thermoelastic – hence reversible – phase transformation between an austenite (A) and a martensite (M) phases. In the austenite phase, a mechanical loading above a critical stress level triggers the nucleation and propagation of the forward phase transformation (A $\rightarrow$ M) and upon unloading below a critical stress level the reverse phase transformation takes place (M $\rightarrow$ A).

Experimental results show that these critical stress levels for phase transformation increase linearly with temperature inside a temperature-stress region known as the Clausius-Clapeyron regime [3, 4]. This linear relation is a critical design parameter, experimentally calculated as being the slope of transformation stress-temperature curves ($d\sigma_{tr}/dT$). This slope is usually known as Clausius-Clapeyron coefficient and is commonly thermodynamically modeled by the Clausius-Clapeyron equation

$$\frac{d\sigma_{tr}}{dT} = -\frac{\rho \Delta S}{\Delta \varepsilon_{tr}} = C \tag{1}$$

where C is the Clausius-Clapeyron coefficient, ρ is the mass density of the transforming material, ΔS is the difference between specific entropies of A and M phases, and $\Delta \varepsilon_{tr}$ is the strain for a complete phase transformation [5, 6].

From a strictly thermodynamic point of view, the Clausius-Clapeyron relation is defined for the thermodynamic equilibrium. It means that the relation in Eq. 1 does not predict any difference between forward and reverse slopes. However, when measured experimentally, a difference between forward and reverse slopes is commonly observed [5, 6] in polycrystalline SMA. This difference is even taken into account in constitutive modeling of SMA thermomechanical behaviour, where two different material parameters are usually attributed for each slope [7, 8]. Despite these evidences, Eq. 1 is always used to thermodynamically model the dependence on temperature of both forward and reverse transformation stresses during superelastic tensile tests.

Other limitation of Eq. 1 is that the only term taking into account the effect of crystallographic configuration, such as texture, is $\Delta\varepsilon_{tr}$. Taking the product of the slopes $d\sigma_{tr}/dT$ by the transformation strain $\Delta\varepsilon_{tr}$, leaves a remaining term equal to the product of mass density ρ and entropy difference ΔS, which depends only on composition [9]. Because the thermoelastic phase transformation in SMA takes place through ordered atomic movement, any significant alignment of crystallographic grains directly affects the mechanical behaviour of the material. Even grain size has been shown to affect the mechanical behaviour of NiTi superelasticity [10, 11].

Many applications of SMA use polycrystalline material in the form of sheets, rods and tubes, all forms that are highly textured [12]. NiTi superelastic thin walled tubes, which are used in the fabrication of 65% of self-expanding cardiovascular stents [13], are highly textured due to their manufacturing process. Barney et al. [14] performed X-ray microdiffractions on micrometric tensile samples cut from a tube in the longitudinal (0°) and circumferential (90°) directions and at 45°. They showed that the mechanical behaviour at 45° greatly differs from the other two studied directions. Likewise, Robertson et al. [12] calculated the theoretical transformation strains of twelve variants of martensite from texture data of drawn tubes. It resulted in the prediction of macro transformation strains in several loading orientations relative to the drawing axis. Their predictions showed that at 45° the transformation strain is smaller than in the lon-

gitudinal and circumferential directions. To the best of the authors' knowledge, no work addresses the anisotropy of the temperature dependence, however.

In this context, this work investigates and analyses the anisotropies of the superelastic behaviour and of its temperature dependence in a thin walled NiTi tube. Firstly, an experimental investigation is carried out in order to address the anisotropy of the thermomechanical behaviour of the tube's material. The original tube is flattened and samples are cut along five orientations from the drawing direction. The samples are submitted to isothermal tensile tests at several temperatures above A_f. The experimental results obtained at each orientation allow the calculation of key SMA properties and a clear quantitative analysis of anisotropy. Afterwards, the observations from this first part are examined from a thermodynamic point of view. This thermodynamic analysis addresses the anisotropy of energy terms involved in a transformation cycle. The anisotropy of the temperature dependence of these energy terms is also analysed, a dependence which is neglected when using the classical Clausius-Clapeyron relation.

2. Material and methods

2.1. NiTi tube and fabrication of tensile samples

A 50.8%atNi-Ti thin walled tube of outer diameter 8.27 mm and wall thickness 0.165 mm was used. This tube was manufactured by Minitubes SA (France). Figure 1 shows a scheme of the fabrication process of the tensile samples, as well as the samples' final dimensions and nomenclature used in this work. The original tube was obtained after the last cold mandrel drawing [15, 16, 17]. A section of this original tube was first cut longitudinally using a pulsed optical fibre laser. This tube section was then flattened through a one-step shape setting at 723 K (450°C) for 20 min in a resistive furnace followed by water quench. The maximum strain to flatten the tube in a "sheet" form was about 1.9% (in absolute value). This is negligible when compared to the strain to which the material is subjected in the manufacturing process of the tube from the ingot. From

the flattened tube, dogbone samples were laser cut in five orientations: $\theta = 0°$ (drawing direction-DD), $\theta = 22.5°$, $\theta = 45°$, $\theta = 67.5°$ and $\theta = 90°$ (transversal direction-TD). The $\vec{e}_y$ and $\vec{e}_x$ directions correspond to the longitudinal and transverse directions of the dogbone samples, respectively.

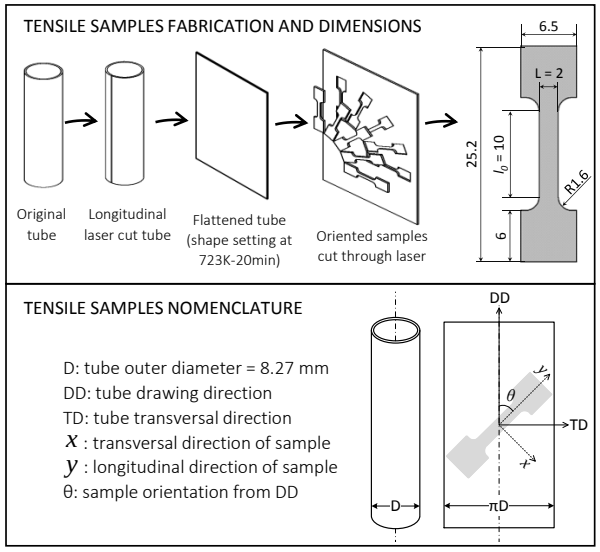

Figure 1: Scheme of fabrication process of dogbone tensile samples from a NiTi tube, the final dimensions of samples and the adopted nomenclature.

Differential Scanning Calorimetry (DSC) analysis (model Q200 from TA Instruments) was performed in samples of both original and flattened tubes. This technique was used to verify the effects of shape setting process in the transformation behaviour of the tube. The analysis was carried out between 373 K and 213 K with a ± 10 K/min rate. Figure 2 presents the DSC results for both original and flattened tubes.

The curve for the original cold-worked tube does not indicate the presence of phase transformation. The curve for the flattened tube presents peaks during cooling and heating. They are associated with Austenite to R-phase transformation (A→R), since little peak energy (≈ 4.3 J/g) and small temperature hysteresis (≈ 5 K) are observed [18, 19]. Transformation temperatures were

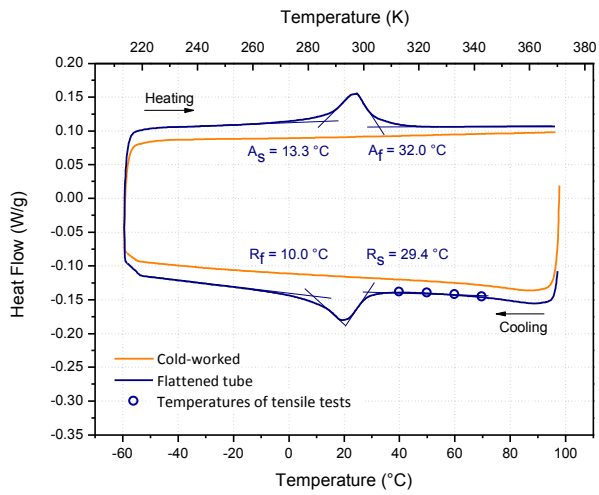

Figure 2: DSC results for the original tube (cold-worked) and for flattened tube (after shape setting at 723 K for 20 min). (In color)

extracted by slope-line-extension method and are: $R_s = 302$ K; $R_f = 283$ K; $A_s = 286$ K; $A_f = 305$ K.

Robertson et al. [12] analyzed the texture of a flattening NiTi tube. They showed that the flattening process, performed through five steps, does not change significantly the texture of the original tube. Moreover, they showed that the texture of the NiTi tube is not altered when the material is submitted to heat treatments. On the contrary, the texture is intensified.

2.2. Isothermal tensile tests

The oriented samples were subjected to isothermal, displacement control tensile tests in a Gabo Eplexor 500N testing machine with a strain rate of 5×10^{-4} s^{-1}. The temperature of the specimen is imposed by a resistive air furnace and controlled by using a fan which blows directly on the specimen. Although the temperature of samples was not measured during tests, tensile results obtained with this strain rate indicate that self-heating was kept to a minimum. This assumption is based in two simultaneous experimental observations: stress plateaus are horizontal and a single, well-defined localization band

(observed in digital image correlation results not shown in this paper) nucleated during tests. Both these observations have been reported in literature to be related with quasi-isothermal experimental conditions, as for example in [20].

Tests were carried out at four temperatures with a measured accuracy of ± 1 K. Testing temperatures were chosen so that at the start of tensile tests samples had an austenite microstructure, based on the DSC results presented in Fig. 2. The chosen temperatures were 313 K (40°C), 323 K (50°C), 333 K (60°C) and 343 K (70°C). After the completion of a superelastic cycle, samples were loaded until rupture. The nominal stress level attained at the end of the superelastic cycle was dependent on the test temperature to allow the sample to attain approximately the same strain level at all temperatures. These stress levels were 750 MPa, 800 MPa, 850 MPa and 900 MPa for the tests at 313 K, 323 K, 333 K and 343 K, respectively. Prior to the isothermal tensile tests, the dogbone samples were heated in boiling water for 1 min, so that all structure was austenitic, and cooled to room temperature to ensure that all samples start tests with the same structure.

The furnace lid contains a transparent crystal window, allowing strain data acquisition through 2-D digital image correlation technique (DIC). The samples were prepared with a black speckle pattern over a white background on their surface. In our study the calculated strain maps correspond to the longitudinal $\varepsilon_{yy}(M)$ component of the Hencky strain tensor in function of the material point M. M is inside a defined zone of interest (ZOI) of around 200 x 1000 pixels. The speckle allowed a 29 px $\times$ 29 px subset to be used in the correlation analysis, performed with Vic2D software from Correlated Solutions. The digital image scale is 0.01 mm/pixel.

To plot the global mechanical behaviour, logarithmic tensile strain ε_{yy} was averaged over the ZOI at each instant. Axial nominal stress is calculated as $\Sigma_{yy} = F/A_0$ where F is the axial force and A_0 is the initial cross section area (A_0 = sample width (L) $\times$ sample thickness = 2 $\times$ 0.165 mm^2). Cauchy (or true) stress is calculated as $\sigma_{yy} = F/A$ where A is the current cross section area. A is obtained from the hypothesis of volume conservation ($A = A_0/\exp(\varepsilon_{yy})$).

3. Thermodynamic framework of thermoelastic martensitic transformation

This section provides a background on the thermodynamic framework used in this work to calculate and discuss some of the analyzed properties. The present approach is based on the works of Ortín and Planes [21, 22, 23] and Wollants et al. [24], Favier and Liu [25] and Liu [26].

This approach is expressed at the scale of a representative element volume (REV). The free energy change dG per unit mass of REV over an infinitesimal step df_m of transformation for a thermoelastic martensitic transformation in a polycrystalline matrix is expressed as [22, 24, 25, 26]:

$$dG = (\Delta H_{ch} - T\Delta S_{ch})df_m + \delta E_{st} + \delta E_{fr} - \delta W^{tr}_{mech} = 0 \tag{2}$$

where:

- f_m is the mass fraction of martensite, defined in the REV. In full austenitic state $f_m = 0$, in full martensitic state $f_m = 1$ and infinitesimal steps df_m are such that $0 \leq f_m \leq 1$;
- ΔH_{ch} is the specific chemical enthalpy of transformation per mass unit of transforming material, understood as the difference between the chemical specific enthalpies of the martensite and austenite phases:

  $\Delta H_{ch} = H^M_{ch} - H^A_{ch}$;
- ΔS_{ch} is the specific chemical entropy of transformation per mass unit of transforming material, understood as the difference between the chemical specific entropies of the martensite and austenite phases:

  $\Delta S_{ch} = S^M_{ch} - S^A_{ch}$;
- T is temperature;
- δE_{st} accounts for the elastic energy stored in the REV by an infinitesimal step df_m of the transformation at the stage corresponding to f_m;

- δE_{fr} accounts for the energy dissipated by the infinitesimal step df_m of transformation at the stage corresponding to f_m;
- δW^{tr}_{mech} represents the external mechanical work per unit mass of the REV required to induce the infinitesimal step of transformation df_m at the same stage.

The occurrence of a stress induced martensitic transformation is determined when the Gibbs free energy of the REV (G) reaches a minimum, which is expressed by the condition ($dG = 0$). In derivative form, this condition results in:

$$G' = \frac{\partial G}{\partial f_m} = \Delta H_{ch} - T\Delta S_{ch} + E'_{st} + E'_{fr} - W^{'tr}_{mech} = 0 \tag{3}$$

where:

- G' is defined by $dG = (\partial G/\partial f_m)df_m = G'df_m$;
- $\delta E_{st} = (\partial E_{st}/\partial f_m)df_m = E'_{st}df_m$;
- $\delta E_{fr} = (\partial E_{fr}/\partial f_m)df_m = E'_{fr}df_m$;
- $\delta W^{tr}_{mech} = (\partial W^{tr}_{mech}/\partial f_m)df_m = W^{'tr}_{mech}df_m$.

In Equation 3, all terms are expressed as energy per unit mass of transforming material in J/kg and are algebraic values. The infinitesimal martensite mass fraction step df_m is positive during forward transformation (austenite to martensite, A→M) and negative during reverse transformation (martensite to austenite, M→A).

The specific chemical **enthalpy and entropy changes**, respectively, ΔH_{ch} and ΔS_{ch}, originate from the difference in atomic arrangement between the two phases. They are both considered constant for a given transformation in a given alloy system. $H^M_{ch} < H^A_{ch}$ and $S^M_{ch} < S^A_{ch}$, leading to $\Delta H_{ch} = H^M_{ch} - H^A_{ch} < 0$ and $\Delta S_{ch} = S^M_{ch} - S^A_{ch} < 0$. Also, the heat capacities of austenite and martensite are assumed equal [24, 27].

The **stored strain energy** term, δE_{st}, includes the elastic energy associated with the accommodation of the shape and volume changes of the transformation. This energy is stored in the system during the forward transformation ($\delta E_{st} > 0$) and progressively released with the reversion of martensite to the parent phase ($\delta E_{st} < 0$). As $df_m > 0$ during forward transformation (A→M) and $df_m < 0$ during reverse transformation (M→A), $E'_{st} > 0$ for both forward and reverse transformations.

The **dissipated energy** term, δE_{fr}, is the sum of all energies consumed during phase transformation. It includes frictional work associated with the moving of internal defects and transformation phase boundaries [24]. As δE_{fr} is always dissipated, its value is always positive for both forward and reverse transformations. As $df_m > 0$ during forward transformation (A→M) and $df_m < 0$ during reverse transformation (M→A), $E'_{fr} > 0$ for the forward transformation and $E'_{fr} < 0$ for the reverse transformation.

The **external mechanical work**, δW^{tr}_{mech}, is expressed as function of the macroscopic strain and stress tensors at the level of the REV, according to continuum mechanics theory. In a tensile test the external mechanical work per unit mass is accounted as $\delta W_{mech} = \frac{1}{\rho}\sigma d\varepsilon$. The volumetric mass density, ρ, is considered in this work as $\rho = 6450$ kg/m^3, σ is the applied tensile Cauchy stress (or true stress) and $d\varepsilon$ is the increment of logarithmic strain. If plastic deformation is negligible, the strain increment can be divided in two summands, an elastic strain increment and a transformation strain increment:

$$d\varepsilon = d\varepsilon_{el} + d\varepsilon_{tr} \tag{4}$$

From this division the external mechanical work can be written as:

$$\delta W_{mech} = \delta W^{el}_{mech} + \delta W^{tr}_{mech} \tag{5}$$

which gives the external mechanical work to induce transformation

$$\delta W^{tr}_{mech} = \frac{1}{\rho}\sigma d\varepsilon_{tr} \tag{6}$$

In this paper, the increment $d\varepsilon_{tr}$ is assumed proportional to the infinitesimal step df_m [28]: $d\varepsilon_{tr} = df_m \Delta\varepsilon_{tr}$, where $\Delta\varepsilon_{tr}$ is the tensile transformation strain for a complete transformation. Thus, $W'^{tr}_{mech} = \frac{1}{\rho}\sigma\Delta\varepsilon_{tr}$. Therefore, for a tensile test, Eq. 3 reads:

$$G' = \Delta H_{ch} - T\Delta S_{ch} + E'_{st} + E'_{fr} - \frac{1}{\rho}\sigma\Delta\varepsilon_{tr} = 0 \tag{7}$$

Equation 7 dictates the energy balance of the thermodynamic system (constituted by the two-phase transforming material) at each σ, T pair. While the specific chemical enthalpy and entropy of transformation are function of composition only, the terms of transformation strain, stored and frictional energies can be function of martensite fraction and temperature.

Now, isolating the tensile Cauchy stress in Eq. 7 one obtains [26]:

$$\sigma = \frac{\rho}{\Delta\varepsilon_{tr}}[\Delta H_{ch} - T\Delta S_{ch} + E'_{st} + E'_{fr}] \tag{8}$$

Differentiating Eq. 8 with respect to temperature gives the general form of the slope of transformation stress-temperature. At a given martensite fraction f_m:

$$\frac{d\sigma}{dT} = \frac{\rho}{\Delta\varepsilon_{tr}}\left(-\Delta S_{ch} + \frac{\partial E'_{st}}{\partial T} + \frac{\partial E'_{fr}}{\partial T}\right) - \frac{\sigma}{\Delta\varepsilon_{tr}}\frac{\partial\Delta\varepsilon_{tr}}{\partial T} \tag{9}$$

The classical Clausius-Clapeyron equation is defined in the thermodynamic equilibrium, i.e. in the absence of any irreversible energy terms and assuming a non temperature dependent transformation strain:

$$\frac{d\sigma}{dT} = -\frac{\rho\Delta S_{ch}}{\Delta\varepsilon_{tr}} = C \tag{10}$$

where C is the Clausius-Clapeyron coefficient for a given phase transformation.

4. Experimental results

Figure 3 contains a set of nominal stress Σ_{yy}-logarithmic ε_{yy} strain curves for five orientations θ and four testing temperatures T. For clarity purposes, the

last loading up to rupture is omitted in this figure and is presented further in the article (see Fig. 6). Perfect superelastic behaviour is observed for all orientations and testing temperatures, with negligible residual strain after unloading.

The curves in Fig. 3 show that the strain achieved at the end of loading varies with orientation, as well as the plateau stress. Unlike the other orientations, it is notable that at $\theta = 45°$ the material does not present a well-defined stress plateau. The absence of a plateau is an indication of a non-localized deformation [29, 30, 31, 32], which was confirmed through the strain maps of DIC.

The testing temperature has little influence on the strain levels. Stress levels increase with increasing testing temperature for all orientations, as expected in NiTi alloys according to the Clausius-Clapeyron relation.

5. Discussion

In this section thermomechanical key properties of NiTi are presented and discussed. A quantitative analysis of the anisotropic behaviour of transformation strain, stress, stress hysteresis and slopes of forward and reverse transformation lines is performed. The methodology used for calculations is presented along with the property itself.

5.1. Qualitative analysis of the anisotropy of mechanical behaviour

From the stress-strain curves of Fig. 3 it is possible to qualitatively infer a strong anisotropy in the mechanical behaviour of the NiTi tube. The strains at the end of loading are very dependent on the orientation. The plateau stresses are also orientation dependent. The overall observation is that the mechanical behaviour evolves almost symmetrically from 0° and 90° directions towards 45°.

The shape of stress-strain curves at 45° from the drawing direction is very distinct compared to the other orientations. Besides reaching the smaller strain at the end of loading, this orientation has a very smooth mechanical behaviour with some degree of hardening. The origin of this distinct mechanical behaviour is attributed to the texture induced by the drawing process of the tube [12,

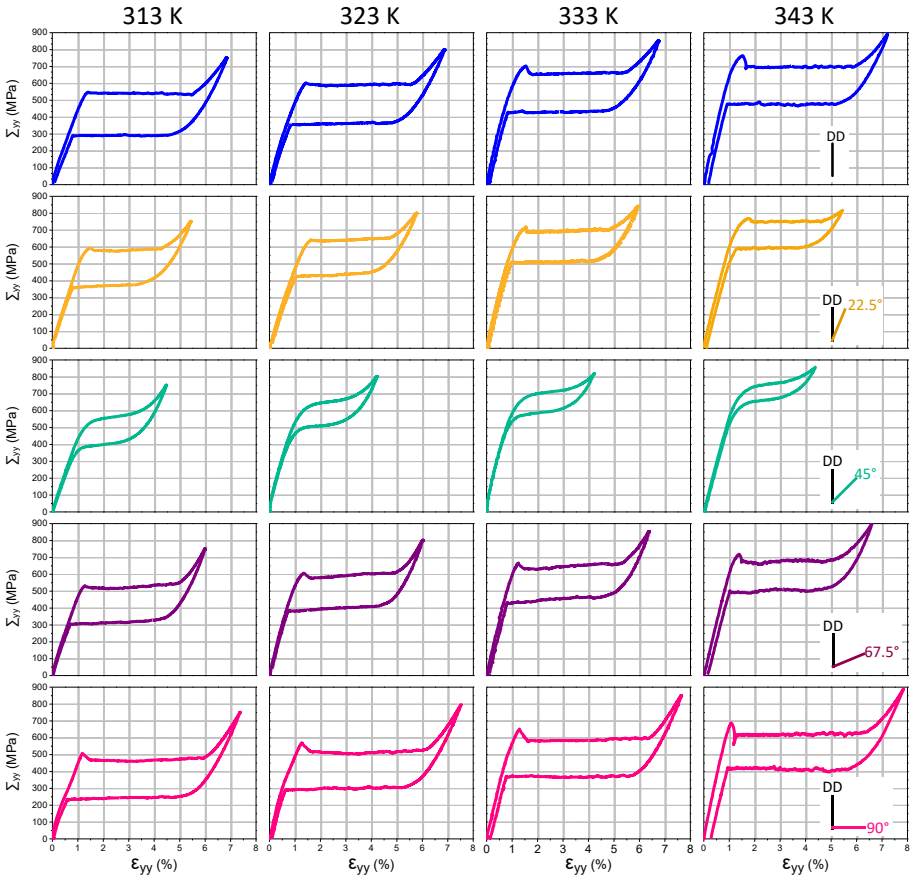

Figure 3: Nominal tensile stress versus logarithmic strain plotted for each orientation at 313 K (40°C), 323 K (50°C), 333 K (60°C) and 343 K (70°C).

33]. Texture measurements performed by Barney et al. [14] in a NiTi tube flattened through a shape setting process show that a specimen cut along the 45° orientation contains predominantly ⟨100⟩-type grains.

Indeed the tensile behaviour of ⟨100⟩ NiTi single crystals measured by Gall et al. [34] resembles those of Fig. 3 for the 45° orientation. The authors show that ⟨100⟩-type grains present strong transformation hardening under tension, which seems to hinder the stress-induced martensitic transformation compared to other single crystal orientations, as well as cause early rupture. Therefore, less transformation strain is observed in this direction.

Another feature of the anisotropy of NiTi tubes observed in the results of Fig. 3 is the symmetrical tendency of mechanical behaviour from 45° orientation towards drawing and transversal directions (0° and 90°). In both senses – from 45° to 0° and from 45° to 90° – the strain at the end of loading increases and the plateau stress decreases for tests at the same temperature. Barney et al. [14] and Bechle and Kyriakides [32] also pointed out the similarities of mechanical behaviour between drawing and transversal directions in NiTi tubes. According to texture measurements, samples cut from thin walled NiTi tubes along the drawing direction have predominantly ⟨111⟩ grains [12, 14], while samples cut along the transversal direction have a mix of ⟨111⟩ and ⟨110⟩-type grains [12]. The tensile tests in NiTi single crystals performed by Gall et al. [34] show that both ⟨111⟩ and ⟨110⟩ grains reach substantial larger strains than ⟨100⟩ grains at the same stress level, besides presenting a well-defined stress plateau.

5.2. Presence of R-phase during tensile tests

As indicated in the DSC results in Fig. 2, the alloy of the tube presents the intermediate R-phase during forward (cooling) and reverse (heating) transformations. Because prior to tensile tests all samples were cooled from 100°C to room temperature (≈ 22°C), samples were introduced in the furnace of the tensile machine with a mixture of R-phase and austenite (DSC peak temperature of A-R transformation is ≈ 20°C). As tensile tests are performed at higher temperatures, the amount of R-phase at the beginning of test decreases. Indeed,

Duerig and Bhattacharya [4, p.495] showed how the presence of the R-phase "plays a critical role in controlling the plateau stress" and pointed out the importance of taking this phase into account when considering stress induced phase transformation.

In the presence of stress, the A↔R transformation is associated with small transformation strains. Literature reports transformation strains between 0.2% and 1% [4, 35], although no information was found concerning the influence of texture or strain orientation. This transformation is noticeable at the apparent elastic zone of the stress-strain curve, with the occurrence of inflection points. In the results of Fig. 3, a slight inflection in initial loading is perceptible for the sample tensioned at 90° at 313 K and 323 K. At higher temperatures, the R-phase vanishes and austenite transforms directly into martensite. In other orientations, this inflection was not observed.

5.3. Anisotropy of the elastic modulus of austenite (E)

The estimation of elastic modulus of a transforming material from a stress-strain curve can be rather inaccurate. This happens because, in addition to pure elasticity, other mechanisms of deformation are involved in the deformation process. In the case of NiTi phase transformation, martensite reorientation [35] and/or plasticity may contribute to lower the measured elastic modulus. Liu and Xiang [36] analysed the measurement of elastic modulus from stress-strain curves of a near-equiatomic NiTi alloy. As a conclusion the authors suggest that the largest value ever measured should be taken as elastic modulus. Nevertheless, the true value of E will always be expected to be greater than the typical measurements from stress-strain curves.

Following this reasoning, the elastic modulus E of the austenite is measured at the very beginning of the true stress (σ_{yy}) versus logarithmic strain ε_{yy} curves at testing temperature $T = 333$ K. This zone has less phase transformation influence. Figure 4b shows the $\sigma_{yy} - \varepsilon_{yy}$ curves (right ordinate axis) at 333 K for all orientations, along with slopes $d\sigma/d\varepsilon$ (left ordinate axis) as a function of strain. Figure 4a shows with more detail the behaviour of $d\sigma/d\varepsilon$ at the beginning

of loading. The elastic modulus at each orientation, E(θ), was determined by plotting $d\sigma/d\varepsilon$ in the range [0.1%, 0.5%] and by extrapolating this value at $\varepsilon_{yy} = 0\%$.

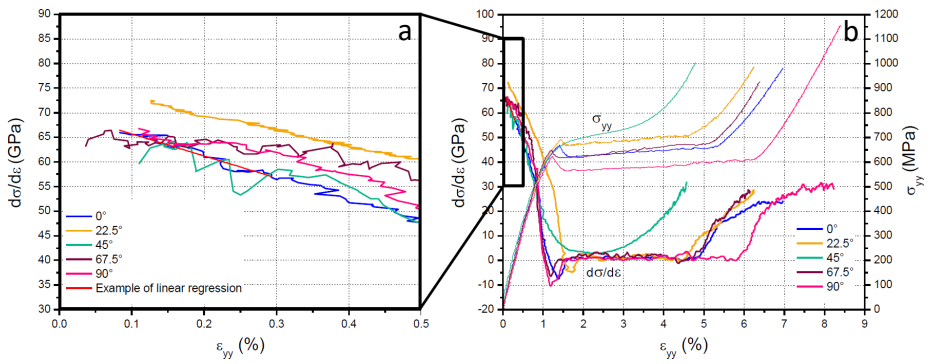

Figure 4: (a) Local slopes $d\sigma/d\varepsilon$ at the beginning of loading for all orientations at T = 333 K, showing the overall tendency when $\varepsilon_{yy} = 0$. (b) $\sigma_{yy} - \varepsilon_{yy}$ behaviour (right axis) and local slopes $d\sigma/d\varepsilon$ (left axis) for the whole strain range. (In color)

Figure 5 shows the extracted E(θ) values. Little orientation dependence is observed. No anisotropy of the austenite elastic modulus of austenite is measured from the results obtained in the present paper.

A mean value of E = 70 GPa is considered and used in this work. This value is a typical elastic modulus value for austenite phase [37, 38]. Bechle and Kyriakides [32] have also reported similar elastic modulus values for austenite phase after performing tensile tests in NiTi tubes: 66.8 GPa and 65.7 GPa for longitudinal and circumferential directions, respectively.

5.4. Inelastic stress-strain curves

Inelastic strain ε_{in} was obtained by subtracting the elastic strain $\varepsilon_{el} = \sigma_{yy}/\mathrm{E}$ from the global mechanical behaviour: $\varepsilon_{in} = \varepsilon_{yy} - \sigma_{yy}/\mathrm{E}$. E is the elastic modulus in the tension direction. It has been shown experimentally in the previous section that for austenite E = 70 GPa for all orientations.

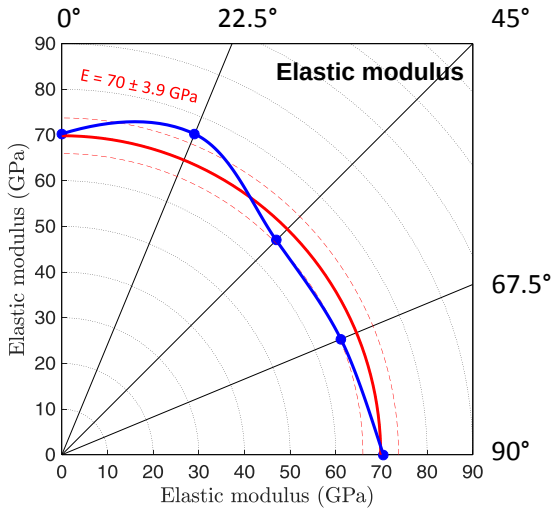

Figure 5: Elastic modulus extracted from tests at 333 K (blue), mean value of 70 GPa (red) and indication of standard deviation of ±3.9 GPa. (In color)

The elastic modulus of oriented martensite is very orientation dependent due to the lower crystal symmetry [39]. The experimental determination of elastic modulus of oriented martensite is however very difficult. In this respect, the work of Alonso et al. (2015, 2019) [37, 38] discusses how tensile stress-strain curves do not provide reliable estimations for the elastic modulus of martensite because of the mixture of deformation mechanisms, even at high stress levels. The authors showed in a rigorous experimental campaign that a reliable method to estimate the elastic modulus of the detwinned martensite formed though stress induced phase transformation is the calculation of the true storage modulus (deduced from the true stress and strain and not from the engineering stress and strain) during a dynamic mechanical analysis performed throughout a superelastic cycle. The martensite modulus should be calculated at stress levels after the stress plateau. Through this method, the elastic modulus of the detwinned martensite phase measures 73 GPa, the same order of magnitude of austenite modulus. The inelastic strain is thus calculated using a elastic modulus E = 70 GPa.

Figure 6 presents the tensile true stress σ_{yy}- logarithmic inelastic ε_{in} strain curves, plotted for each testing temperature, including loading until rupture for tests at 313 K, 323 K and 333 K. Except for plateau stress, the overall behaviour of all samples is similar for all temperatures. Some cycling effect was observed between the first and second loadings but mainly in the stress level and practically negligible on strain.

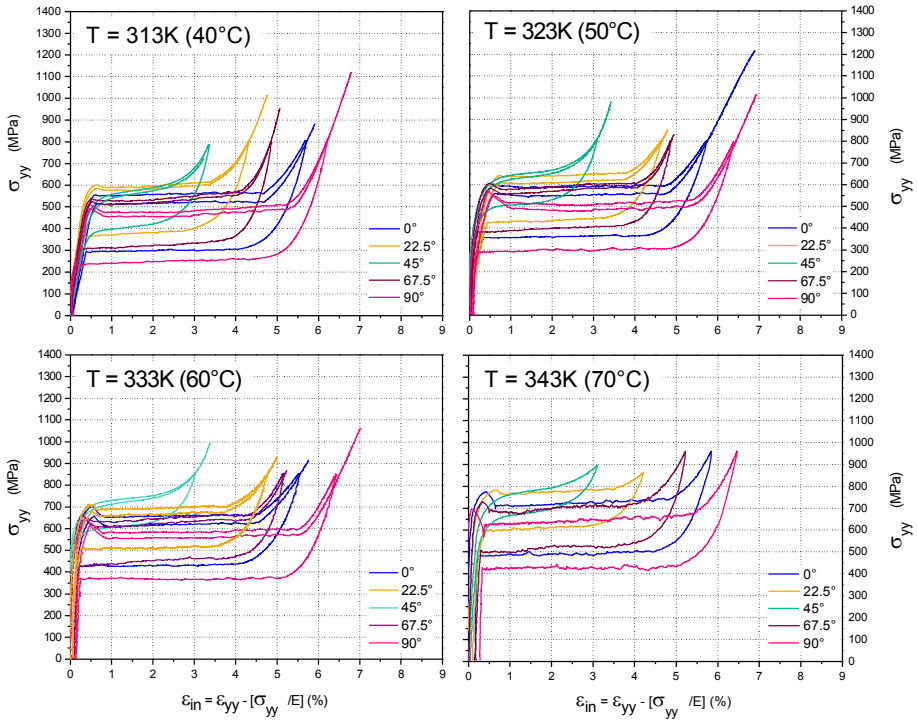

Figure 6: True tensile stress versus inelastic strain curves as function of testing temperature. (In color)

5.5. *Anisotropy of the transformation strain ($\Delta\varepsilon_{tr}$)*

Among the different methods to measure transformation strain, the plateau strain — which is simply the length of the stress plateau in a stress-strain curve — has been a very recurrent method used for superelastic alloys. However, the plateau strain is not a measure of the total transformation strain [4]. It is in fact

associated with the deformation of only the most favourably oriented martensite variants. In order to complete phase transformation the less favourably oriented variants still need to transform. This takes place as the stress resumes increasing, right after the plateau [40]. In other words, the phase transformation is still taking place outside the stress plateau region [31].

There are other evidences that martensitic transformation completion does not coincide with the end of stress plateau [30, 31, 40]. One work in particular, by Pelton et al. [28], shows that at the end of macroscopic stress plateau the martensite fraction has reached around 85%. These measurements were performed with neutron diffraction technique, which allows to compute the behaviour of the bulk material.

Therefore, instead of the plateau strain, transformation strains ($\Delta\varepsilon_{tr}$) were determined from the σ_{yy}- logarithmic ε_{in} strain loading curves until rupture, plotted in Fig. 6. The procedure to estimate $\Delta\varepsilon_{tr}$ is based on the following:

- It was considered that there is a region of the loading curve after the stress plateau for which no plastic strain was experienced by the samples. Two facts give support to this assumption. On one hand, no residual strain was observed after unloading; it means that there is no plastic deformation for strains lower than the maximum strain of the superelastic cycle. On the other hand, seen the trend of loading curves until rupture in 6, it is likely that negligible plastic strain was experienced by the samples. The fact that the $d\sigma/d\varepsilon$ slope is still increasing at the end of loading for all orientations (see Fig. 4b) is also an indication of the absence of plastic deformation. This is consistent with the amount of cold-work to which the tube was submitted during manufacturing process. Moreover, the $\sigma_{yy} - \varepsilon_{in}$ curves do not show any change of curvature between the end of stress plateau and the rupture point (except for the sample $\theta = 0°$ tested at 323 K).

- Elastic moduli of austenite and detwinned martensite are equal when true stress is used [41, 37, 38]. With equal austenite and martensite elastic modulus, when the material completes transformation (martensite fraction

$f_m = 1$) in the absence of plasticity, the $\sigma_{yy} - \varepsilon_{in}$ curves would tend to a vertical line outside the zone of the stress plateau.

- Because of that, the function in Equation 11 was used to fit the final portion of the $\sigma_{yy} - \varepsilon_{in}$ curve between a point P and the rupture point, as schematically illustrated in Fig. 7.

$$\varepsilon_{in} - \varepsilon_P = (\Delta\varepsilon_{tr} - \varepsilon_P) \tanh\left(a \frac{\sigma_{yy} - \sigma_P}{\Delta\varepsilon_{tr} - \varepsilon_P}\right) \tag{11}$$

The tanh function was chosen because it reaches smoothly a constant value. σ_P, ε_P and a are the true stress, inelastic strain and local slope at point P, respectively.

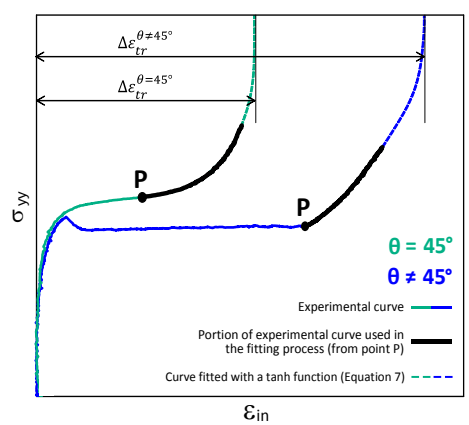

Figure 7: Methodology used for the estimation of total transformation strain from curves of loading until rupture, which can be applied with or without the presence of a stress plateau. (In color)

Figure 8 shows the result of fitting for all orientations and testing temperatures.

Figure 9a shows the dependence of $\Delta\varepsilon_{tr}$ on orientation, determined using the previous methodology.

The following observations can be made regarding the orientation and temperature dependencies:

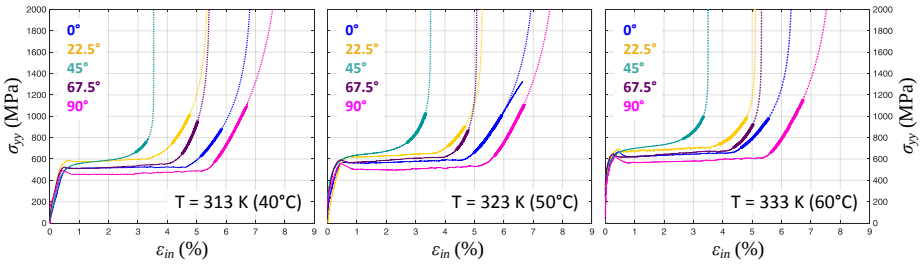

Figure 8: Results of fittings with Equation 11 for estimation of transformation strains ($\Delta\varepsilon_{tr}$). The thick zones are the final portions of the $\sigma_{yy} - \varepsilon_{in}$ curves that were used in the fitting process. (In color)

- $\Delta\varepsilon_{tr}$ is mostly independent of the testing temperature for all directions. The highest difference occurred at 0°, with standard deviation of only 4%.

- Because of that, mean values of $\Delta\varepsilon_{tr}$ are considered for each orientation and were plotted with a thicker line. A very strong anisotropy is observed. This anisotropy is almost symmetric with direction 45° as "mirror direction". The greatest difference reaches 58%, between 45° and 90°.

Based on the works of Robertson et al. [33], Robertson et al. [12] and Barney et al. [14] (as discussed in section 5.1), tensile specimens cut from NiTi tubes at 0°, 45° and 90° have grains predominantly oriented at $\langle 111 \rangle$, $\langle 100 \rangle$ and a mix of $\langle 111 \rangle$ and $\langle 110 \rangle$ directions, respectively. Thus, the transformation strain results in Fig. 9a can be compared with results of solutionized NiTi single crystals tensioned in the [100], [110] and $[\bar{1}11]$ crystallographic directions of Miyazaki et al. [42] (inverse pole figure in Fig. 9b). Indeed a similar trend of total transformation strain is observed between polycrystalline 0°, 45°, 90° samples and $\langle 111 \rangle$, $\langle 100 \rangle$, $\langle 110 \rangle$ single crystals.

Moreover, a similar dependence was found experimentally by Robertson et al. [12] for a flattened NiTi tube with 0.7 mm of wall thickness. However, the authors do not present their experimental curves and consider the transformation strain as the strain attained at the end of the stress plateaus. They also comment on how this shape of $\Delta\varepsilon_{tr} - \theta$ curve is consistent with paths of fatigue

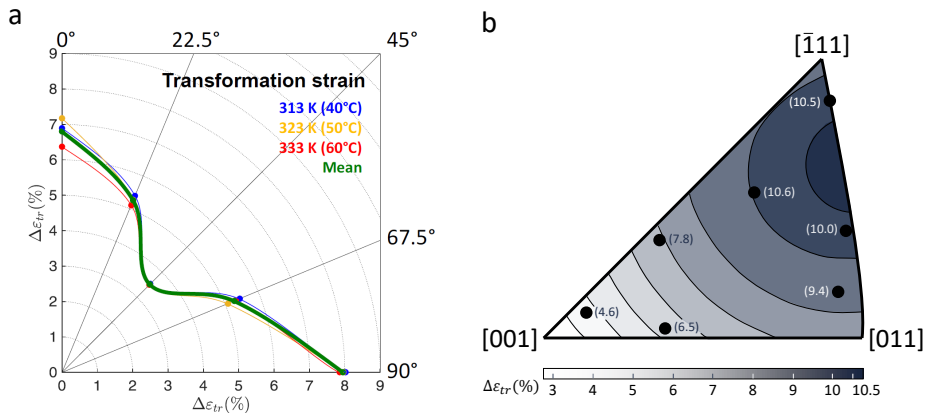

Figure 9: (a) Transformation strain ($\Delta\varepsilon_{tr}$) values for all orientations and tested temperatures. (b) Inverse pole figure showing the orientation dependence of the recoverable strain of solution-treated single crystals (parenthesis) and calculated values (contour lines) (From [42]). (In color)

cracks in NiTi tubes, which preferentially follow the 45° direction, the direction that "requires the lowest strain energy to form martensite".

5.6. Anisotropy of forward and reverse transformation stresses

When a stress strain curve has a well defined stress plateau, the transformation stresses are generally defined as being the stress levels of the plateaus. The stress-strain results presented in Fig. 3, however, show that the superelastic material of the tube can have behaviours with or without plateau, depending on the orientation. Then, for comparison purposes, the procedure for obtaining the transformation stresses had to be standardized.

The method used in this work was to measure the transformation stresses σ_{tr} at the same level of martensite fraction. Forward and reverse transformation stresses were then extracted at $\varepsilon_{in} = \Delta\varepsilon_{tr}(\theta)/2$, where $\Delta\varepsilon_{tr}(\theta)$ is the total transformation strain of each orientation. This is hypothetically equivalent to $f_m = 0.5$, assuming a linear relation between inelastic strain and martensite fraction f_m [43].

Figure 10a presents the variation of σ_{tr} for forward and reverse transformations with θ for all testing temperatures. The overall trend of the curves is an increase of σ_{tr} from 0° to 45° followed by a decrease from 45° to 90°. However, less anisotropy is observed for the stresses for forward (F) than for reverse (R) transformation.

This difference between loading and unloading implies that it exists an anisotropy in the stress hysteresis. The stress hysteresis, defined as $\sigma_{tr}^{hys} = \sigma_{tr}^{F} - \sigma_{tr}^{R}$ was calculated from the data in Fig. 10a and is shown in Fig. 10b. σ_{tr}^{hys} is smaller at 45° and higher at 0° and 90°.

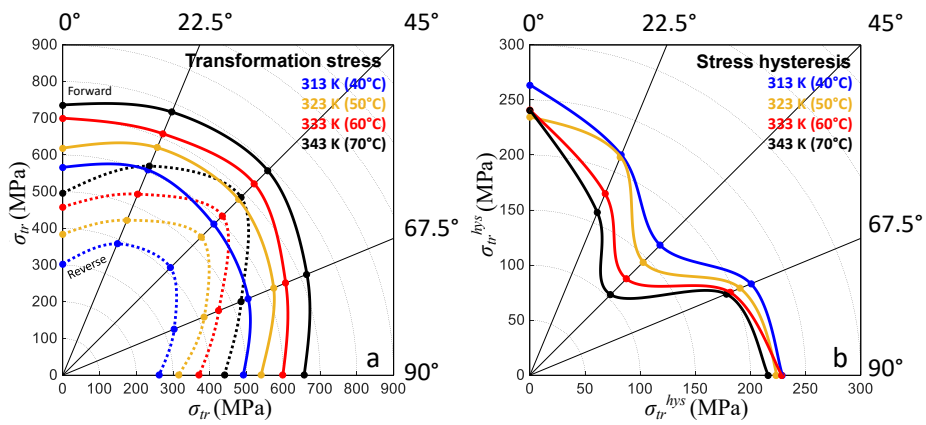

Figure 10: (a) Polar plot of transformation stresses at loading (forward transformation, F) and unloading (reverse transformation, R) defined at $f_m = 0.5$. (b) Stress hysteresis, calculated as the difference between transformation stress of loading and unloading ($\sigma_{tr}^{hys} = \sigma_{tr}^{F} - \sigma_{tr}^{R}$). (In color)

In stress-induced phase transformation the hysteresis observed is caused mostly by dissipative processes which are associated mainly to the frictional work due to interfacial motion [44]. Indeed, Barney et al. [14] showed that tensile loading at the 45° orientation leaves behind islands of untransformed material due to its predominant texture. Based on this, it is possible that the more restricted lattice movement in the 45° sample could hinder the interfacial

motion. The restricted movement at 45° is caused by its probable predominant grain orientation, as discussed in Section 5.1. Therefore, less energy dissipation and smaller hysteresis were observed in this sample compared to other orientations.

5.7. Anisotropy of transformation lines slopes ($d\sigma_{tr}/dT$)

Figure 11 shows the forward and reverse transformation stresses as function of the temperature for the five orientations. In order to determine the errors on the transformation stresses, several tests were repeated (they are not shown in this paper for clarity purpose). They allowed to estimate an error bar of ±20 MPa for the determination of the transformation stress. The solid segments connect two successive transformation stresses. The dashed lines are obtained by performing a linear regression for the four tested temperatures. For all orientations, the slopes of the forward and reverse solid segments are not temperature dependent and are close to the slopes of the forward and reverse dashed lines, respectively.

In order to suppress the effect of the R-phase, it would be better to calculate the slopes for temperatures higher than 60°C, i.e. using only the results at 60°C and 70°C. However the accuracy of the slope calculated using only two temperatures would be very low, of the order of ±2MPa/K. Due to these observations, lines slopes $d\sigma_{tr}/dT$ were calculated for each orientation using the four available transformation stresses for forward and reverse transformations as being the slopes of the dashed lines of Fig. 11.

Figure 12 shows the transformation lines slopes for all orientations. A strong anisotropy is observed. The slope at $\theta = 0°$ is comparable to the Clausius-Clapeyron coefficient of austenite-martensite transformation of NiTi wires (≈ 6 MPa/K) [4]. Wires typically present a $\langle 111 \rangle$ texture [45, 46], which is the predominant texture in the drawing direction of NiTi tubes [12].

Besides the anisotropy of forward and reverse slopes, two other behaviours are observed:

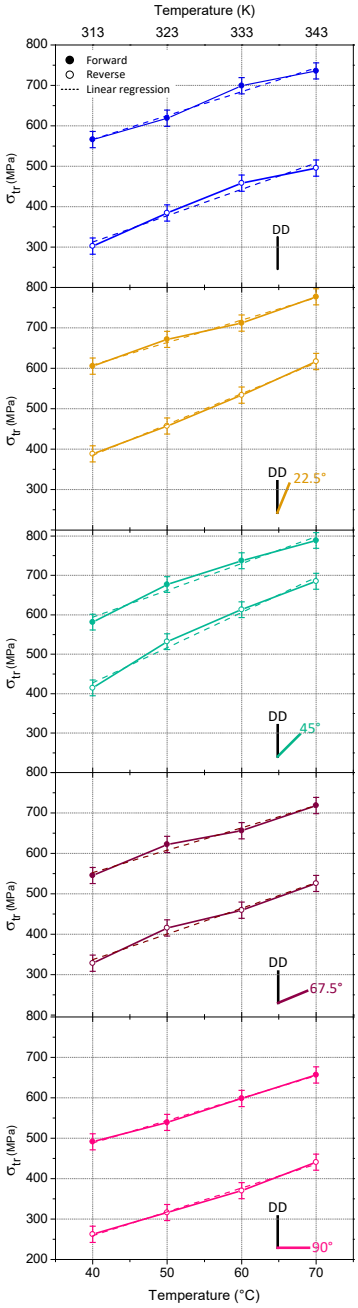

Figure 11: Forward (load) and reverse (unload) transformation stresses as a function of test temperature for all tested orientations. The dashed lines are obtained by performing a linear regression for the four tested temperatures. (In color)

- $d\sigma_{tr}/dT$ for forward transformation is always smaller than $d\sigma_{tr}/dT$ for reverse transformation;
- the difference between forward and reverse slopes is very anisotropic.

These observations are discussed in more detail in Section 6 in a thermodynamic analysis.

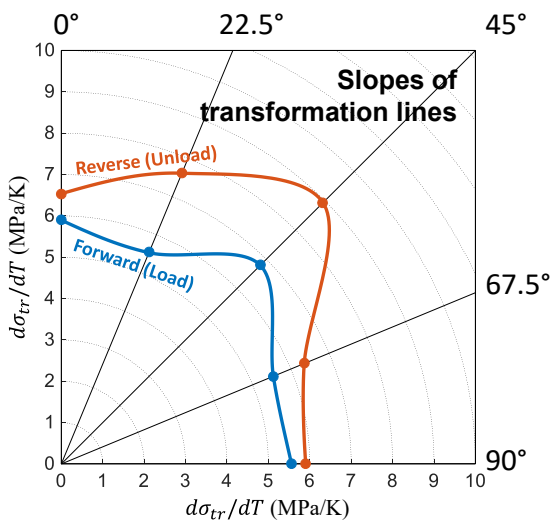

Figure 12: Slopes of transformation lines for forward and reverse transformations at $f_m = 0.5$. (In color)

6. Thermodynamic analysis of the anisotropy

The experimental results are analysed using the thermodynamic framework presented in Section 3.

6.1. Orientation dependence of the product $(d\sigma_{tr}/dT)\Delta\varepsilon_{tr}$

Equation 10 states the relation between external stress and temperature usually applied for a thermoelastic phase transformation. This form of the Clausius-Clapeyron equation is widely used for SMA. If this equation applies, the product $(d\sigma_{tr}/dT)\Delta\varepsilon_{tr}$ should neither depend on orientation, neither be

different for forward and reverse transformations. This is because the entropy change ΔS_{ch} and mass density ρ depend only on the alloy composition [9].

However, observing the experimental curves in Fig. 13, the product of slopes of transformation lines and $\Delta\varepsilon_{tr}$ is in fact very orientation dependent and different between loading and unloading. This result can be analyzed considering the relation written in Eq. 9. It has been shown in Fig. 9a that for all directions the transformation strain $\Delta\varepsilon_{tr}$ is not dependent on temperature. Thus the fact that the product $(d\sigma_{tr}/dT)\Delta\varepsilon_{tr}$ is not constant indicates that the stored and frictional energies might be temperature dependent.

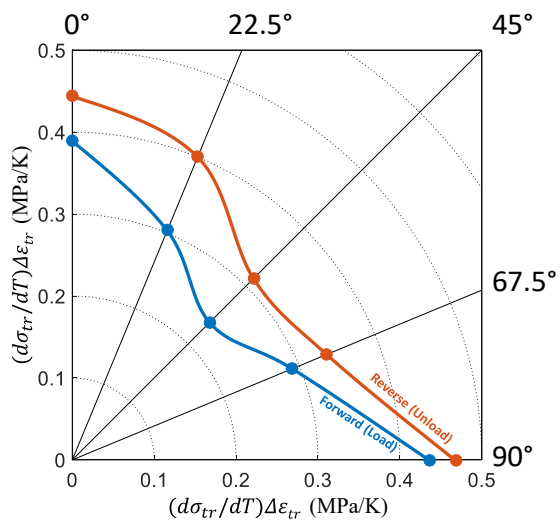

Figure 13: Product of the slopes of the transformation lines by transformation strains, showing an orientation dependent behaviour. (In color)

6.2. Temperature dependence of frictional work and stored elastic energy

In order to investigate the temperature dependence of the frictional work and stored elastic energy terms, let us consider Eq. 8. Re-writing it for the forward (F) and reverse (R) transformations separately, gives respectively:

$$\sigma_{tr}^{F}(f_m, T) = \frac{\rho}{\Delta\varepsilon_{tr}}[\Delta H_{ch} - T\Delta S_{ch} + E_{st}^{'F}(f_m, T) + E_{fr}^{'F}(f_m, T)] \tag{12}$$

with $E_{st}^{'F}(f_m,T) > 0$ and $E_{fr}^{'F}(f_m,T) > 0$;

$$\sigma_{tr}^{R}(f_m,T) = \frac{\rho}{\Delta\varepsilon_{tr}}[\Delta H_{ch} - T\Delta S_{ch} + E_{st}^{'R}(f_m,T) + E_{fr}^{'R}(f_m,T)] \tag{13}$$

with $E_{st}^{'R}(f_m,T) > 0$ and $E_{fr}^{'R}(f_m,T) < 0$.

Subtracting Eq. 13 from Eq. 12 one obtains:

$$\begin{aligned}(\sigma_{tr}^{F} - \sigma_{tr}^{R})_{(f_m,T)} &= \frac{\rho}{\Delta\varepsilon_{tr}}[(E_{st}^{'F} + E_{fr}^{'F}) - (E_{st}^{'R} + E_{fr}^{'R})]_{(f_m,T)} \\ &= \frac{\rho}{\Delta\varepsilon_{tr}}\Delta E'(f_m,T)\end{aligned} \tag{14}$$

Equation 14 states that $(\sigma_{tr}^{F}-\sigma_{tr}^{R})_{(f_m,T)}$ is directly proportional to $\Delta E'(f_m,T)$. This term accounts for the difference of specific irreversible energies between forward and reverse austenite-martensite transformations, which can be written:

$$\Delta E'(f_m,T) = (E_{st}^{'F} - E_{st}^{'R}) + (E_{fr}^{'F} + \mid E_{fr}^{'R} \mid) \tag{15}$$

where $\mid E_{fr}^{'R} \mid$ is the absolute value of the frictional energy of reverse transformation, adopted to make explicit the sign of this term, avoiding any ambiguity.

The dependence of $\Delta E'(f_m,T)$ with temperature is analysed for the specimens cut along 45° from the drawing direction. The mechanical behaviour in this orientation does not experience the localization phenomenon and thus the martensite fraction dependence can also be evaluated. Figure 14b illustrates the behaviour of $\Delta E'(f_m,T)$ calculated using Eq. 14. To the most part $\Delta E'$ does not depend on f_m. It clearly depends on temperature, though. Figure 14c shows graphically $\Delta E'(T)$ as function of test temperature, calculated as mean values in the f_m range where it is constant. For $\theta = 45°$ $\Delta E'$ decreases linearly with increasing temperature with a rate of -0.012 J g^{-1} K^{-1}. This dependence on temperature is generally neglected, especially if the classic Clausius-Clapeyron equation is used.

An hypothesis for the negative temperature dependence of the irreversible energy is that the temperature increase is accompanied by the increase of trans-

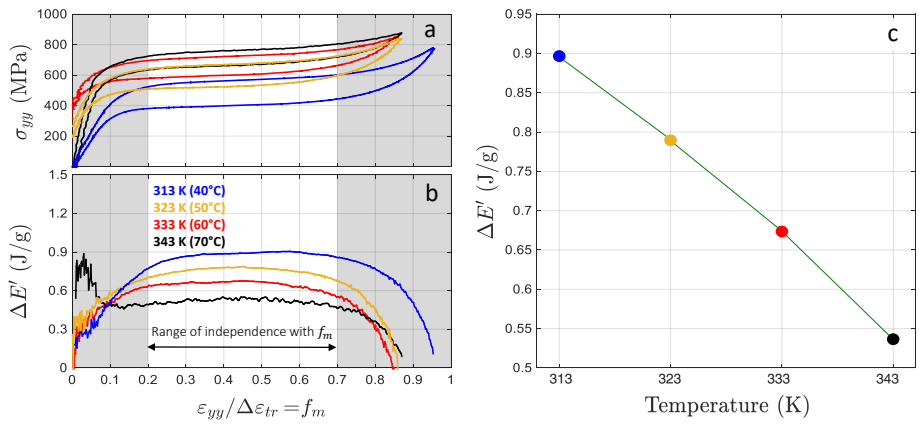

Figure 14: (a) True stress versus estimated martensite fraction at different temperatures for specimens cut along $\theta = 45°$. (b) Difference between loading and unloading stresses plotted in (a). (c) Temperature dependence of the term $\Delta E'$ extracted from (b) as the mean value in the range of independence with f_m. (In color)

formation stress, due to the Clausius-Clapeyron relation. With the increase of applied stress, less martensite variants might form, or in other words, the growth of martensite variants that are better aligned with the applied stress is favored. This higher crystallographic alignment likely leads to less frictional energy loss during phase transformation. Analogously, during mechanical cycling, where crystallographic alignment is induced by loading, it is observed a drop in the value of stored elastic energy and frictional energy [47].

6.3. Origin of the difference between forward and reverse slopes of transformation lines

The consequences of the aforementioned temperature dependence on the difference between slopes of transformation lines are now analysed. Equation 9 is written for the forward and reverse transformations in Eq. 16 and Eq. 17, respectively. Since transformation strain does not depend on temperature, this

term is neglected hereafter.

$$\left(\frac{d\sigma}{dT}\right)^F = \frac{\rho}{\Delta\varepsilon_{tr}}\left(-\Delta S_{ch} + \frac{\partial E_{st}^{'F}}{\partial T} + \frac{\partial E_{fr}^{'F}}{\partial T}\right) \tag{16}$$

$$\left(\frac{d\sigma}{dT}\right)^R = \frac{\rho}{\Delta\varepsilon_{tr}}\left(-\Delta S_{ch} + \frac{\partial E_{st}^{'R}}{\partial T} - \frac{\partial \left|E_{fr}^{'R}\right|}{\partial T}\right) \tag{17}$$

Subtracting $(d\sigma_{tr}/dT)^R$ from $(d\sigma_{tr}/dT)^F$ (Eq. 16 minus Eq. 17) one gets:

$$\left(\frac{d\sigma}{dT}\right)^F - \left(\frac{d\sigma}{dT}\right)^R = \frac{\rho}{\Delta\varepsilon_{tr}}\left[\frac{\partial(E_{st}^{'F} + E_{fr}^{'F})}{\partial T} - \frac{\partial(E_{st}^{'R} - \mid E_{fr}^{'R} \mid)}{\partial T}\right] \tag{18}$$

According to Eq. 14, the term inside the square brackets in Eq. 18 is equal to:

$$\frac{\partial \Delta E'}{\partial T} = \frac{\partial(E_{st}^{'F} - E_{st}^{'R})}{\partial T} + \frac{\partial(E_{fr}^{'F} + \mid E_{fr}^{'R} \mid)}{\partial T} \tag{19}$$

From Eq. 18 and Eq. 19, the difference between $(d\sigma_{tr}/dT)^F$ and $(d\sigma_{tr}/dT)^R$ is caused by the fact that $\partial\Delta E'/\partial T \neq 0$.

As shown in Fig. 12, $(d\sigma_{tr}/dT)^F < (d\sigma_{tr}/dT)^R$ for all orientations. This difference is commonly observed in NiTi alloys and some authors have attempted to explain it. Liu and Yang [6], concluded that $(d\sigma_{tr}/dT)^F < (d\sigma_{tr}/dT)^R$ because the transformation strain is bigger for loading (F) than for unloading (R). Thus, as the slope of stress-temperature transformation lines are inversely proportional to transformation strain, $(d\sigma_{tr}/dT)^F < (d\sigma_{tr}/dT)^R$. However, they consider the transformation strains to be the lengths of forward and reverse stress plateaus. This premise is somewhat amiss, since it has been found evidence that martensitic transformation completion does not coincide with the end of the plateau [30, 31]. In our opinion, the transformation strain is equal for forward and reverse transformations and then the explanation suggested by Liu and Yang [6] would not be valid. The presented experimental results and the performed thermodynamic analysis show that $\partial\Delta E'/\partial T \neq 0$ is a more thermodynamically reasonable explanation for $(d\sigma_{tr}/dT)^F \neq (d\sigma_{tr}/dT)^R$.

Furthermore, as stated in Eq. 18 and Eq. 19, the nature of the relation between $\Delta E'$ and temperature determines the relation between $(d\sigma_{tr}/dT)^F$ and $(d\sigma_{tr}/dT)^R$: since $\partial\Delta E'/\partial T < 0$ (see Fig. 14c), $(d\sigma_{tr}/dT)^F < (d\sigma_{tr}/dT)^R$.

6.4. Anisotropy of the temperature dependences of the stored and frictional energies

Figure 13 shows that the products $(d\sigma_{tr}/dT)\Delta\varepsilon_{tr}$ are different for forward and reverse transformations and that the difference is orientation dependent. It is concluded that $\partial\Delta E'/\partial T$ is also orientation dependent.

In Eq. 16 and Eq. 17 the temperature dependencies of the irreversible energies for forward and reverse transformations are four unkowns and thus it is not possible to calculate these four terms individually. Nevertheless, assuming that the temperature dependencies of the forward and reverse stored energy are equal:

$$\frac{\partial E'_{st}}{\partial T} = \frac{\partial E'^{F}_{st}}{\partial T} = \frac{\partial E'^{R}_{st}}{\partial T} \tag{20}$$

$$\frac{\partial E'_{fr}}{\partial T} = \frac{\partial E'^{F}_{fr}}{\partial T} = \frac{\partial \left| E'^{R}_{fr} \right|}{\partial T} \tag{21}$$

it is possible to calculate the total irreversible energies for a thermodynamic cycle by adding and subtracting Eq. 16 and Eq. 17. Taking into account Equations 20 - 21 and performing some algebraic manipulation, the stored and frictional energy temperature dependencies are:

$$\frac{\partial E'_{st}}{\partial T} = \frac{1}{2}\frac{\Delta\varepsilon_{tr}}{\rho}\left[\left(\frac{d\sigma}{dT}\right)^F + \left(\frac{d\sigma}{dT}\right)^R\right] + \Delta S_{ch} \tag{22}$$

$$\frac{\partial E'_{fr}}{\partial T} = \frac{1}{2}\frac{\Delta\varepsilon_{tr}}{\rho}\left[\left(\frac{d\sigma}{dT}\right)^F - \left(\frac{d\sigma}{dT}\right)^R\right] \tag{23}$$

Figure 15 shows the result of Eq. 22 and Eq. 23 calculated using experimental data of Fig. 9 and Fig. 12 with $\rho = 6450$ kg/m^3. The error bars in the

graph indicate the sensibility of dE'_{st}/dT to ΔS_{ch} values. For a 50.8%atNi-Ti alloy, the interval $60.5 \leq \Delta S_{ch} \leq 63$ J/gK was used [48].

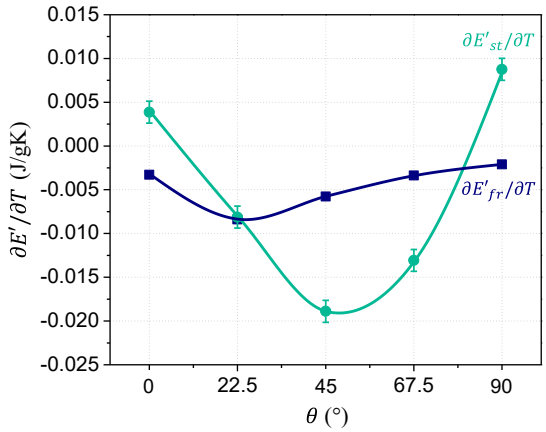

Figure 15: Temperature dependencies of stored and dissipated energies as function of the orientation. The error bars indicate stored elastic energy values calculated with $60.5 \leq \Delta S_{ch} \leq 63$ J/gK for a 50.8%atNi-Ti alloy [48]. (In color)

Figure 15 show a strong orientation dependence, mainly for the stored elastic energy. Multiplying the values in Figure 15 by the applied temperature difference ($\Delta T = 30°$C) shows that $\Delta E'_{st}$ and $\Delta E'_{fr}$ are between 0.1 and 0.6 J/g, which are within the range found for this material [47, 49].

7. Conclusion

The anisotropy of the temperature dependence of superelastic SMA was studied through the experimental characterization and thermomechanical analysis of transformation stresses and strains in a thin walled NiTi tube. From the experimental data, the following conclusions are drawn:

1. In the studied temperature range (from 40°C to 70°C), full transformation strain depends strongly on orientation but not on temperature. The lowest transformation strains were measured at 45° from the drawing direction. An almost symmetric profile was observed from this orientation

to the drawing (0°) and transversal directions (90°). Variations of transformation strain reached 58% between orientations.

2. Transformation stress is also anisotropic. However, stress for reverse transformation is more orientation dependent than for forward transformation.
3. Slopes of the transformation stress-temperature lines of forward and reverse transformations are significantly anisotropic. Besides, the slope for reverse transformation is higher than for forward transformation for all orientations.

Supported by our experimental data, the following conclusions are achieved concerning the thermodynamic analysis:

1. The temperature dependence of the difference of specific irreversible energy is not negligible as assumed by the classical Clausius-Clapeyron equation, typically used to model both forward and reverse slopes of the transformation stress-temperature lines. This conclusion is drawn based on the fact that the product of slopes of the transformation stress-temperature lines and total transformation strain strongly depends on orientation.
2. Irreversibilities of the phase transformation are due to specific stored elastic energy (E'_{st}) and specific frictional energy (E'_{fr}). The difference $\Delta E'$ of the irreversible energy ($E'_{st} + E'_{fr}$) between loading (forward F transformation) and unloading (reverse R transformation) of a superelastic test decreases with increasing test temperature.
3. The dependence of $\Delta E'$ on temperature is the cause for the slopes of the forward and reverse transformation stress-temperature lines to be different. For the studied material, $\partial \Delta E'/\partial T$ is negative, leading to a $d\sigma_{tr}/dT$ smaller for forward transformation than for the reverse transformation.
4. The dependence of $\Delta E'$ on temperature is also orientation dependent. Indeed, the temperature dependencies of both stored and dissipated specific energies are orientation dependent.

Acknowledgments

This work was conducted during a scholarship (248892/2013-4) supported by the Ciências Sem Fronteiras Program at the University of Grenoble, financed by the Brazilian National Council for Scientific and Technological Development (CNPq).

References

[1] D. C. Lagoudas. *Shape Memory Alloys: modeling and engineering applications*. Springer, Boston, MA, 2008. ISBN 978-0-387-47685-8. doi: https://doi.org/10.1007/978-0-387-47685-8. URL `https://link.springer.com/book/10.1007/978-0-387-47685-8`.

[2] J. M. Jani, M. Leary, A. Subic, and M. A. Gibson. A review of shape memory alloy research, applications and opportunities. *Materials & Design*, 56:1078–1113, apr 2014. ISSN 02613069. doi: 10.1016/j.matdes.2013.11.084. URL `http://linkinghub.elsevier.com/retrieve/pii/S0261306913011345`.

[3] K. Otsuka and K. Shimizu. Pseudoelasticity and shape memory effects in alloys. *International Metals Reviews*, 31(1):93–114, 1986. ISSN 0308-4590. doi: 10.1179/imtr.1986.31.1.93. URL `http://www.maneyonline.com/doi/abs/10.1179/imtr.1986.31.1.93`.

[4] T. W. Duerig and K. Bhattacharya. The measurement and interpretation of transformation temperatures in nitinol. *ASM International - International Conference on Shape Memory and Superelastic Technologies, SMST 2017*, 2017-May(4):204–205, 2017. ISSN 2199-3858. doi: 10.1007/s40830-017-0133-0.

[5] Y. Liu, A. Mahmud, F. Kursawe, and T. Nam. Effect of pseudoelastic cycling on the Clausius – Clapeyron relation for stress-induced martensitic

transformation in NiTi. *Journal of Alloys and Compounds*, 449:82–87, 2008. doi: 10.1016/j.jallcom.2006.02.080.

[6] Y. Liu and H. Yang. Strain dependence of the Clausius–Clapeyron relation for thermoelastic martensitic transformations in NiTi. *Smart Materials and Structures*, 16(1):S22–S27, 2007. ISSN 0964-1726. doi: 10.1088/0964-1726/16/1/S03. URL `http://stacks.iop.org/0964-1726/16/i=1/a=S03`.

[7] A. R. Damanpack, M. Bodaghi, and W. H. Liao. A Finite-Strain Constitutive Model for Anisotropic Shape Memory Alloys. *Mechanics of Materials*, 2017. ISSN 01676636. doi: 10.1016/j.mechmat.2017.05.012. URL `http://linkinghub.elsevier.com/retrieve/pii/S0167663616302770`.

[8] B. Zhou. A macroscopic constitutive model of shape memory alloy considering plasticity. *Mechanics of Materials*, 48:71–81, may 2012. ISSN 01676636. doi: 10.1016/j.mechmat.2012.02.001. URL `http://linkinghub.elsevier.com/retrieve/pii/S0167663612000233`.

[9] J. Frenzel, A. Wieczorek, I. Opahle, B. Maaß, R. Drautz, and G. Eggeler. On the effect of alloy composition on martensite start temperatures and latent heats in Ni-Ti-based shape memory alloys. *Acta Materialia*, 90:213–231, 2015. ISSN 13596454. doi: 10.1016/j.actamat.2015.02.029. URL `http://dx.doi.org/10.1016/j.actamat.2015.02.029`.

[10] C. Yu, G. Kang, X. Xie, and W. Rao. A micromechanical model for the grain size dependent super-elasticity degeneration of NiTi shape memory alloys. *Mechanics of Materials*, 125:35–51, 2018. ISSN 01676636. doi: 10.1016/j.mechmat.2018.07.008. URL `https://doi.org/10.1016/j.mechmat.2018.07.008`.

[11] Q. Sun, A. Aslan, M. Li, and M. Chen. Effects of grain size on phase transition behavior of nanocrystalline shape memory alloys. *Science China Technological Sciences*, 57(4):671–679, 2014. ISSN 1862281X. doi: 10.1007/s11431-014-5505-5.

[12] S. W. Robertson, X. Y. Gong, and R. O. Ritchie. Effect of product form and heat treatment on the crystallographic texture of austenitic Nitinol. *Journal of Materials Science*, 41:621–630, 2006. ISSN 00222461. doi: 10.1007/s10853-006-6478-y.

[13] C. Bonsignore. A Decade of Evolution in Stent Design. In Alan R Pelton and T. W. Duerig, editors, *Proceedings of the International Conference on Shape memory and Superelastic Technologies*, Pacific Grove, California, USA, 2004. doi: 10.1361/cp2003smst519.

[14] M. M. Barney, D. Xu, S. W. Robertson, V. Schroeder, R. O. Ritchie, A. R. Pelton, and A. Mehta. Impact of thermomechanical texture on the superelastic response of Nitinol implants. *Journal of the mechanical behavior of biomedical materials*, 4(7):1431–9, oct 2011. ISSN 1878-0180. doi: 10.1016/j.jmbbm.2011.05.013. URL `http://www.ncbi.nlm.nih.gov/pubmed/21783153`.

[15] D. Favier, Y. Liu, L. Orgéas, A. Sandel, L. Debove, and P. Comte-Gaz. Influence of thermomechanical processing on the superelastic properties of a Ni-rich Nitinol shape memory alloy. *Materials Science and Engineering A*, 429(1-2):130–136, 2006. ISSN 09215093. doi: 10.1016/j.msea.2006.05.018.

[16] M. Palengat, G. Chagnon, D. Favier, H. Louche, C. Linardon, and C. Plaideau. Cold drawing of 316L stainless steel thin-walled tubes : Experiments and finite element analysis. *International Journal of Mechanical Sciences*, 70:69–78, 2013. ISSN 0020-7403. doi: 10.1016/j.ijmecsci.2013.02.003. URL `http://dx.doi.org/10.1016/j.ijmecsci.2013.02.003`.

[17] C. Linardon, D. Favier, G. Chagnon, and B. Gruez. A conical mandrel tube drawing test designed to assess failure criteria. *Journal of Materials Processing Tech.*, 214(2):347–357, 2014. ISSN 0924-0136. doi: 10.1016/j.jmatprotec.2013.09.021. URL `http://dx.doi.org/10.1016/j.jmatprotec.2013.09.021`.

[18] T. Saburi. Ti-Ni shape memory alloys. In K. Otsuka and C. M. Wayman, editors, *Shape Memory Materials*, chapter 3, pages 49–96. Cambridge University Press, 1998. ISBN 9780521663847. URL `https://www.cambridge.org/br/academic/subjects/engineering/materials-science/shape-memory-materials?format=PB{&}isbn=9780521663847`.

[19] Y. Zheng, F. Jiang, L. Li, H. Yang, and Y. Liu. Effect of ageing treatment on the transformation behaviour of Ti–50.9at.% Ni alloy. *Acta Materialia*, 56(4):736–745, 2008. ISSN 13596454. doi: 10.1016/j.actamat.2007.10.020.

[20] C. Elibol and M. F.X. Wagner. Strain rate effects on the localization of the stress-induced martensitic transformation in pseudoelastic NiTi under uniaxial tension, compression and compression-shear. *Materials Science and Engineering A*, 643:194–202, 2015. ISSN 09215093. doi: 10.1016/j.msea.2015.07.039. URL `http://dx.doi.org/10.1016/j.msea.2015.07.039`.

[21] J. Ortín and A. Planes. Thermodynamics and Hysteresis Behaviour of Thermoelastic Martensitic Transformations. *Le Journal de Physique IV*, 01(C4):13–23, 1991. ISSN 1155-4339. doi: 10.1051/jp4:1991402. URL `http://www.edpsciences.org/10.1051/jp4:1991402`.

[22] J. Ortín and A. Planes. Thermodynamics of Thermoelastic Martensitic Transformations. *Acta Metallurgica*, 37(5):1433–1441, 1989. doi: 10.1016/0001-6160(89)90175-2.

[23] J. Ortín and A. Planes. Thermodynamic analysis of thermal measurements in thermoelastic martensitic transformations. *Acta Metallurgica*, 36 (8):1873–1889, 1988. ISSN 00016160. doi: 10.1016/0001-6160(88)90291-X.

[24] P. Wollants, J. R. Roos, and L. Delaey. Thermally and stress-induced thermoelastic martensitic transformations in the reference frame of equilibrium thermodynamics. *Progress in Materials Science*, 37:227–288, 1993. doi: 10.1016/0079-6425(93)90005-6.

[25] D. Favier and Y. Liu. Restoration by rapid overheating of thermally stabilised martensite of NiTi shape memory alloys. *Journal of Alloys and Compounds*, 297(1-2):114–121, 2000. ISSN 09258388. doi: 10.1016/S0925-8388(99)00576-9.

[26] Y. Liu. Thermodynamics of the shape memory effect in NiTi alloys. In Takayuki Yoneyama and Shuichi Miyazaki, editors, *Shape Memory Alloys for Biomedical Applications*, chapter 3, pages 37–67. Woodheadn Publishing, 2009. ISBN 9781845693442.

[27] V. Delobelle. *Contribuitions à l'étude thermomécanique des alliages à memoire de forme NiTi et à la réalisation par soudage e matériaux architecturés NiTi*. PhD thesis, Université de Grenoble, 2012.

[28] A. R. Pelton, B. Clausen, and A. P. Stebner. In Situ Neutron Diffraction Studies of Increasing Tension Strains of Superelastic Nitinol. *Shape Memory and Superelasticity*, 1(3):375–386, 2015. ISSN 2199-384X. doi: 10.1007/s40830-015-0031-2. URL `http://link.springer.com/10.1007/s40830-015-0031-2`.

[29] D Favier and L. Orgéas. Stress-induced transformation of a NiTi alloy in isothermal shear, tension and compression. *Acta Materialia*, 46(15):5579–5591, 1998.

[30] P. Šittner, Y. Liu, and V. Novak. On the origin of Lüders-like deformation of NiTi shape memory alloys. *Journal of the Mechanics and Physics of Solids*, 53(8):1719–1746, aug 2005. ISSN 00225096. doi: 10.1016/j.jmps.2005.03.005. URL `http://linkinghub.elsevier.com/retrieve/pii/S0022509605000712`.

[31] D. Favier, H. Louche, P. Schlosser, L. Orgéas, P. Vacher, and L. Debove. Homogeneous and heterogeneous deformation mechanisms in an austenitic polycrystalline Ti-50.8 at.% Ni thin tube under tension. Investigation via temperature and strain fields measurements. *Acta Materialia*, 55(16):5310–5322, 2007. ISSN 13596454. doi: 10.1016/j.actamat.2007.05.027.

[32] N. J. Bechle and S. Kyriakides. Evolution of localization in pseudoelastic NiTi tubes under biaxial stress states. *International Journal of Plasticity*, 82:1–31, 2016. ISSN 07496419. doi: 10.1016/j.ijplas.2016.01.017.

[33] S. W. Robertson, V. Imbeni, H. R. Wenk, and R. O. Ritchie. Crystallographic texture for tube and plate of the superelastic/shape- memory alloy Nitinol used for endovascular stents. *Journal of Biomedical Materials Research - Part A*, 72(2):190–199, 2005. ISSN 00219304. doi: 10.1002/jbm.a.30214.

[34] K. Gall, H. Sehitoglu, Y. I. Chumlyakov, and I. V. Kireeva. Tension-compression asymmetry of the stress-strain response in aged single crystal and polycrystalline NiTi. *Acta Materialia*, 47(4):1203–1217, 1999. ISSN 13596454. doi: 10.1016/S1359-6454(98)00432-7.

[35] P. Šittner, M. Landa, P. Lukáš, and V. Novák. R-phase transformation phenomena in thermomechanically loaded NiTi polycrystals. *Mechanics of Materials*, 38(5-6):475–492, 2006. ISSN 01676636. doi: 10.1016/j.mechmat.2005.05.025. URL `http://linkinghub.elsevier.com/retrieve/pii/S0167663605001225`.

[36] Y. Liu and H. Xiang. Apparent modulus of elasticity of near-equiatomic NiTi. *Journal of Alloys and Compounds*, 270:154–159, 1998. ISSN 09258388. doi: 10.1016/S0925-8388(98)00500-3.

[37] T. Alonso. *Caracterisation par essais DMA et optimisation du comportement thermomecanique de fils de NiTi - Application a une aiguille medicale deformable*. PhD thesis, Université Grenoble Alpes, 2015.

[38] T. Alonso, D. Favier, and G. Chagnon. Characterizing transformation phenomena and elastic moduli of austenite and oriented martensite of superelastic thin NiTi wire through isothermal Dynamic Mechanical Analysis. *Journal of Materials Engineering and Performance*, pages 2–28, 2019. doi: 10.1002/ente.20)).

[39] Ashley N. Bucsek, Harshad M. Paranjape, and Aaron P. Stebner. Myths and Truths of Nitinol Mechanics: Elasticity and Tension–Compression Asymmetry. *Shape Memory and Superelasticity*, 2(3):264–271, 2016. ISSN 21993858. doi: 10.1007/s40830-016-0074-z.

[40] Y. Liu. The superelastic anisotropy in a NiTi shape memory alloy thin sheet. *Acta Materialia*, 95:411–427, apr 2015. ISSN 13596454. doi: 10.1016/j.actamat.2015.03.022. URL `http://linkinghub.elsevier.com/retrieve/pii/S1359645415001895`.

[41] M. F. Wagner and W. Windl. Lattice stability , elastic constants and macroscopic moduli of NiTi martensites from first principles. *Acta Materialia*, 56:6232–6245, 2008. doi: 10.1016/j.actamat.2008.08.043.

[42] S. Miyazaki, S. Kimura, K. Otsuka, and Y. Suzuki. The habit plane and transformation strains associated with the martensitic transformation in Ti-Ni single crystals. *Scripta Metallurgica*, 18(9):883–888, 1984. ISSN 00369748. doi: 10.1016/0036-9748(84)90254-0.

[43] A. P. Stebner, H. M. Paranjape, B. Clausen, L. C. Brinson, and A. R. Pelton. In Situ Neutron Diffraction Studies of Large Monotonic Deformations of Superelastic Nitinol. *Shape Memory and Superelasticity*, 1(2):252–267, 2015. ISSN 2199-3858. doi: 10.1007/s40830-015-0015-2.

[44] R. F. Hamilton, H. Sehitoglu, Y. I. Chumlyakov, and H. J. Maier. Stress dependence of the hysteresis in single crystal NiTi alloys. *Acta Materialia*, 52:3383–3402, 2004. doi: 10.1016/j.actamat.2004.03.038.

[45] G. Laplanche, T. Birk, S. Schneider, J. Frenzel, and G. Eggeler. Effect of temperature and texture on the reorientation of martensite variants in NiTi shape memory alloys. *Acta Materialia*, 127:143–152, 2017. ISSN 13596454. doi: 10.1016/j.actamat.2017.01.023. URL `http://dx.doi.org/10.1016/j.actamat.2017.01.023`.

[46] Ken Gall, Jeff Tyber, Valerie Brice, Carl P. Frick, Hans J. Maier, and Neil Morgan. Tensile deformation of NiTi wires. *Journal of Biomedical Materials Research - Part A*, 75(4):810–823, 2005. ISSN 00219304. doi: 10.1002/jbm.a.30464.

[47] P. G. McCormick and Yinong Liu. Thermodynamic analysis of the martensitic transformation in NiTi-II. Effect of transformation cycling. *Acta Metallurgica Et Materialia*, 42(7):2407–2413, 1994. ISSN 09567151. doi: 10.1016/0956-7151(94)90319-0.

[48] Jafar Khalil-Allafi and Behnam Amin-Ahmadi. The effect of chemical composition on enthalpy and entropy changes of martensitic transformations in binary NiTi shape memory alloys. *Journal of Alloys and Compounds*, 487 (1-2):363–366, 2009. ISSN 09258388. doi: 10.1016/j.jallcom.2009.07.135.

[49] Qinglin Meng, Hong Yang, Yinong Liu, and Tae Hyun Nam. Transformation intervals and elastic strain energies of B2-B19′ martensitic transformation of NiTi. *Intermetallics*, 18(12):2431–2434, 2010. ISSN 09669795. doi: 10.1016/j.intermet.2010.08.038. URL `http://dx.doi.org/10.1016/j.intermet.2010.08.038`.